Rotational population transfer through the $A\,^2\Pi_u$-$X\,^2\Sigma_g^+$-$B\,^2\Sigma_u^+$ coupling in N_2^+ lasing

Youyuan Zhang,[1] Erik Lötstedt,[1] Toshiaki Ando,[1] Atsushi Iwasaki,[1] Huailiang Xu,[2,3] and Kaoru Yamanouchi[1,*]

[1]*Department of Chemistry, School of Science, The University of Tokyo, 7-3-1 Hongo, Bunkyo-ku, Tokyo 113-0033, Japan*

[2]*State Key Laboratory of Integrated Optoelectronics, College of Electronic Science and Engineering, Jilin University, Changchun 130012, China*

[3]*CAS Center for Excellence in Ultra-intense Laser Science, Shanghai 201800, China*

(Received 7 May 2021; accepted 4 August 2021; published 19 August 2021)

The lasing of N_2^+ at 391 nm, originating from the population inversion between $X\,^2\Sigma_g^+(v=0)$ and $B\,^2\Sigma_u^+(v=0)$ achieved by the irradiation of a pair of few-cycle intense near-IR laser pulses in a pump-probe scheme, is investigated both experimentally and theoretically. The characteristic periodic intensity modulations recorded experimentally in both *P*- and *R*-branch emission lines are reproduced well by the theoretical simulation, in which the population transfer processes among the rovibrational levels of the three lowest electronic states, $X\,^2\Sigma_g^+$, $A\,^2\Pi_u$, and $B\,^2\Sigma_u^+$, of N_2^+ induced by pump and probe few-cycle intense laser pulses are calculated. Based on the results of the theoretical simulation, the periodic intensity modulations are ascribed to the difference between the rotational selection rules in the $A\,^2\Pi_u$-$X\,^2\Sigma_g^+$ coupling, which suppresses the rotational excitation in the $X\,^2\Sigma_g^+(0)$ state, and those in the $B\,^2\Sigma_u^+$-$X\,^2\Sigma_g^+$ coupling, which enhances the rotational excitation in the $B\,^2\Sigma_u^+(0)$ state.

DOI: 10.1103/PhysRevA.104.023107

I. INTRODUCTION

When near-IR intense ultrashort laser pulses are focused into air, a coherent and unidirectional radiation at 391 nm is generated [1–10]. This phenomenon, called air lasing, has been an attractive research subject in the past two decades because of the complex lasing mechanism. This radiation at 391 nm corresponds to the emission from the vibrational ground state of the electronically excited $B\,^2\Sigma_u^+$ state, which is hereafter called the $B(0)$ state, to the vibrational ground $X\,^2\Sigma_g^+$ state, which is hereafter called the $X(0)$ state, of N_2^+. Therefore, in order that the $B(0)$-$X(0)$ lasing occurs, the population in the $B(0)$ state is expected to be larger than that in the $X(0)$ state, that is, the population inversion is expected to be realized. However, because the photon energy of the near-IR laser field of a Ti:sapphire laser at 800 nm is only one-half of the photon energy required to transfer the population in the $X(0)$ state to the $B(0)$ state through the $B(0)$-$X(0)$ transition, it was considered that such a simple optical pumping within a near-IR laser field could not explain the air lasing phenomenon, and thus many different schemes have been proposed to explain the lasing phenomena [8,11–19].

Xu *et al.* [4] proposed a mechanism of population inversion between the $B(0)$ state and the $X(0)$ state and demonstrated by numerical calculations that the population inversion of N_2^+ is realized within a near-IR ultrashort laser pulse so that the air lasing at 391 nm is realized. In the mechanism, N_2^+ created by the ionization in the laser field is suddenly exposed to the remaining part of the intense laser field so that the population in the $X(0)$ state is transferred to the $B(0)$ state and almost simultaneously the population in the $X(0)$ state is further transferred to the low vibrational levels in the electronically excited $A\,^2\Pi_u$ state within the remaining part of the ultrashort laser pulse (see Fig. 1). A similar mechanism was also proposed by Yao *et al.* [5].

Later, Xu *et al.* [6] performed the air lasing experiment combined with the alignment of N_2 and showed that the lasing intensity is enhanced at every rotational revival time when the N-N molecular axis becomes parallel to the polarization of the probe laser pulse, which was regarded as evidence that the rotational degrees of freedom play an important role in the air lasing phenomenon. It was further demonstrated by Li *et al.* [21] that the polarization-modulated ultrashort laser pulse within which the laser polarization direction rotates enhances significantly the air lasing at 391 nm, showing that the population in the $X(0)$ state N_2^+ is efficiently depleted by the $A(v)$-$X(0)$ transition within the remaining part of the ultrashort laser pulse after N_2^+ is created by the ionization.

Firm evidence of the involvement of the *A*-*X* transition was reported by the Fourier transform of the lasing signal at 391 nm [22]. It was demonstrated that the intensity of the $B(0)$-$X(0)$ lasing is modulated with the frequencies corresponding to the $A(v)$-$X(0)$ transitions, showing that the three-state *A*-*X*-*B* coupling proceeds within the laser field to generate the air lasing. Very recently, it was shown both experimentally and theoretically that an additional IR pulse at 1.6 μm can deplete the population in the $X(0)$ state almost completely via the vibrational Raman pumping so that the air lasing intensity is enhanced by five to six orders of magnitude [23].

On the other hand, the so-called sudden turn-on mechanism was examined for a two-level system by a Floquet picture [24] and it was revealed that the sudden turn-on of the laser

*kaoru@chem.s.u-tokyo.ac.jp

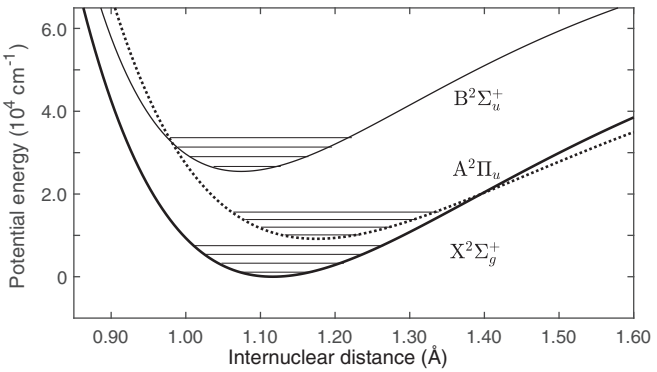

FIG. 1. Potential energy curves of the three electronic states $X\,^2\Sigma_g{}^+$, $A\,^2\Pi_u$, and $B\,^2\Sigma_u{}^+$ of $N_2{}^+$ [20]. The $A\,^2\Pi_u$-$X\,^2\Sigma_g{}^+$ and $B\,^2\Sigma_u{}^+$-$X\,^2\Sigma_g{}^+$ transitions are dipole allowed and the $B\,^2\Sigma_u{}^+$-$A\,^2\Pi_u$ transition is dipole forbidden.

pulse induces a population transfer from the lower level to the upper level even when the photon energy is only one-half of the energy gap between the two levels. The Floquet analysis was also performed for the air lasing of $N_2{}^+$ [25] and it was revealed that the sudden turn-on of the laser field combined with the *A*-*X* pumping efficiently enhances the population inversion.

So far, we have learned that the air lasing at 391 nm can be explained well by the sudden turn-on model combined with the *A*-*X*-*B* coupling in $N_2{}^+$. In our recent theoretical study on the air lasing in which the rotational degrees of freedom are explicitly included in the three-state coupling model [4,6,24], it was revealed that the population inversion can be achieved between the rotationally excited levels, leading to the air lasing even when the net population in the $B(0)$ state is not inverted with respect to the net population in the $X(0)$ state [26]. Indeed, several experimental reports [15,22,27] have been made on the importance of the rotational excitation in the air lasing at 391 nm.

Rotational excitation in the air lasing at 391 nm has been reported [28–31], and the population inversion between the specific rotational states in the $X\,^2\Sigma_g{}^+$ and $B\,^2\Sigma_u{}^+$ states was identified experimentally using near-IR (800-nm) laser pulses [15]. On the other hand, using a pump-probe scheme, it was reported that population inversion can be achieved between specific rotational levels [27] at a specific pump-probe delay time through the resonant coupling between the $X\,^2\Sigma_g{}^+$ and $B\,^2\Sigma_u{}^+$ states induced by a 391-nm probe pulse even when the population inversion is not achieved by a pump pulse. By a similar pump-seed scheme, the loss and gain in the *P* and *R* branches of the 391-nm emission were investigated to discuss the rotational excitation in the $X\,^2\Sigma_g{}^+$ state of $N_2{}^+$ [19]. It is therefore worth examining how the populations in the rotational levels in the three electronic states are transferred to each other in an intense laser field, leading to the rotationally enhanced air lasing. A recent experimental study showed that the rotational wave packet is formed only in the *B* state of $N_2{}^+$ and that no rotational coherence is observed in the *X* state [32].

In the present study, in order to clarify the role of the rotational degrees of freedom in the air lasing, we perform pump-probe measurements of the rotational structure of the emission spectrum of the $B(0)$-$X(0)$ lasing and a theoretical simulation of the population transfer among the rovibronic levels of the $X\,^2\Sigma_g{}^+$, $A\,^2\Pi_u$, and $B\,^2\Sigma_u{}^+$ states of $N_2{}^+$ in which the rotational degrees of freedom are explicitly included. Furthermore, we show that the selection rules of the rotational quantum number *K* and the differences between the rovibronic transition intensities between the *B*-*X* and *A*-*X* transitions play a crucial role in the creation of the rotationally inverted populations between the $B(0)$ and $X(0)$ states through the creation of the rotational coherence in the $B(0)$ state.

II. EXPERIMENT: ROTATIONALLY RESOLVED PUMP-PROBE MEASUREMENTS

A. Experimental setup

The details of the pump-probe measurements were described in Ref. [22]. Briefly, the few-cycle intense NIR laser pulses were generated from the output of a Ti:sapphire laser system by the pulse compression technique with a hollow-core fiber and chirped mirrors. The pulse duration was measured to be 7 fs. The few-cycle intense laser pulses were introduced into the Michelson interferometer to prepare the pump (40 μJ) and probe (20 μJ) pulses. The delay time was scanned by an optical stage in the interferometer with a time step of approximately 0.2 fs. The two laser pulses were focused by a parabolic mirror ($f = 50$ mm) into a gas cell filled with nitrogen gas at 150 mbar. In order to estimate the focal intensity of the laser pulses, the focal size was measured using a CCD camera after the pulse energy was attenuated, and the focal intensities of the pump and probe laser pulses were estimated to be 6.6×10^{14} and 3.3×10^{14} W/cm^2, respectively. Because the focal size of the laser pulse creating the filament is expected to be larger than the measured focal size by the plasma defocusing effect, the estimated field intensities can be regarded as upper limits of the laser intensity in the filament. The forwardly propagating light was introduced into a fiber spectrometer (Ocean optics USB 4000-UV-VIS) by a focusing lens ($f = 30$ mm) after the spectral component of the fundamental laser light, whose wavelength is longer than 450 nm, was removed using a bandpass filter and a dielectric mirror having a high reflectivity at 800 nm.

B. Experimental results

The experimental emission spectrum recorded as a function of the pump-probe delay time Δt is shown in Fig. 2(a). In the observed emission spectrum, the emission peak of the *P*-branch head (labeled *P*) appears at around 391.5 nm in the entire delay time range. On the other hand, the two separated series of the *R*-branch emission peaks (labeled *R*1 and *R*2) appear in the wavelength below 390 nm. The *R*1 branch starts appearing at around $\Delta t = 120$ fs and $\lambda = 389$ nm and its intensity maximum moves towards the longer wavelength region until *R*1 fades out at around $\Delta t = 280$ fs and $\lambda = 390$ nm. In turn, the *R*2 branch starts appearing at around $\Delta t = 250$ fs and $\lambda = 388.5$ nm and its intensity maximum moves towards the longer wavelength region until *R*2 reaches $\Delta t = 500$ fs and $\lambda = 389$ nm.

In addition, a fine oscillation with a period of 13–20 fs, corresponding to a frequency range of 50–75 THz, can be clearly

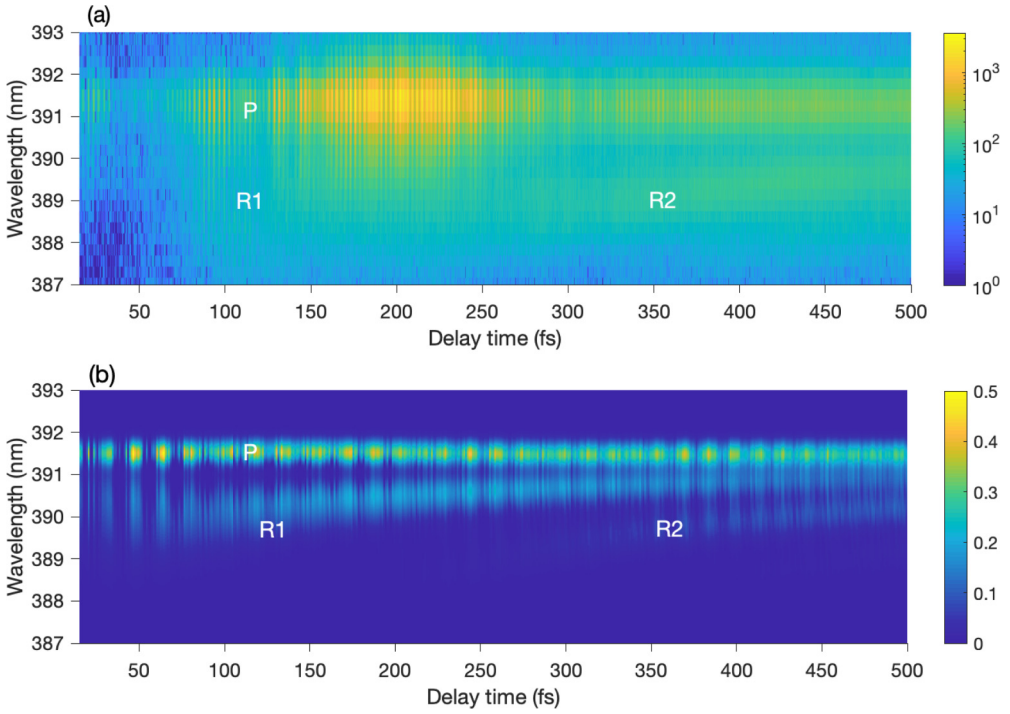

FIG. 2. (a) Experimental and (b) theoretical emission spectra of N_2^+ plotted as a function of the pump-probe delay time. The intensity of the emission is shown in a logarithmic color scale. The spectral resolution in (b) is set to $t = 0.2$ nm, which is 7.5 times better than that in (a) (FWHM equal to 1.5 nm), so that the time evolution of the spectral structure can be seen clearly.

identified in the P-branch head emission at around 391.5 nm. This oscillation appearing in the P-branch head emission was assigned to the energy separations of the vibrational levels in the three lowest-lying electronic states of $X\,^2\Sigma_g^+$, $A\,^2\Pi_u$, and $B\,^2\Sigma_u^+$ of N_2^+ based on the Fourier transform analysis of the P-branch head emission [22]. A similar fine oscillation with a period of 13–20 fs can also be identified in the emission intensities of the $R1$ and $R2$ branches. The finer oscillations can be assigned to the energy separations of the vibrational levels between the $A\,^2\Pi_u$ and $X\,^2\Sigma_g^+$ states [22].

III. THEORY

A. Theoretical model of the pump-probe process

In order to simulate the excitation process of N_2^+, we express a linearly polarized pump laser pulse $\mathcal{E}_{\rm pump}(t)$ as

$$\mathcal{E}_{\rm pump}(t) = \mathcal{E}^{\rm peak}_{\rm pump} f_{\rm pump}(t)\cos(\omega t), \tag{1}$$

where ω is the frequency of the laser pulse and $f_{\rm pump}(t)$ represents a half-Gaussian envelope function defined as

$$f_{\rm pump}(t) = \begin{cases} e^{-t^2/2\sigma_0^2} & \text{for } t \geqslant 0 \\ 0 & \text{for } t < 0, \end{cases} \tag{2}$$

whose full width at half maximum is $\tau_{\rm FWHM} = 2\sqrt{2\ln 2}\sigma_0$. The simulation starts from $t = 0$ because the tunneling ionization most preferentially occurs at the peak amplitude of the laser pulse [26]. At the delay time Δt with respect to the pump pulse, we introduce a linearly polarized probe laser pulse $\mathcal{E}_{\rm probe}(t)$ given by

$$\mathcal{E}_{\rm probe}(t) = \mathcal{E}^{\rm peak}_{\rm probe} f_{\rm probe}(t-\Delta t)\cos[\omega(t-\Delta t)], \tag{3}$$

where $f_{\rm probe}(t)$ represents a full-Gaussian envelope function given by

$$f_{\rm probe}(t) = e^{-t^2/2\sigma_0^2}. \tag{4}$$

The delay time Δt is defined as the delay time of the intensity peak of the probe laser pulse with respect to the intensity peak of the pump laser pulse at $t = 0$. The polarization direction of the probe laser pulse is set parallel to the polarization direction of the pump laser pulse.

In the simulation, an initial state is mapped to a final state using the S matrices representing the pump and probe processes as

$$\hat{c}_{\rm final} = S_{\rm probe} T S_{\rm pump} \hat{c}_{\rm initial}, \tag{5}$$

where $\hat{c}_{\rm initial}$ is a column vector of the coefficients for the rovibronic states in the three electronic states at $t = 0$, $\hat{c}_{\rm final}$ is a column vector of the coefficients for the final rovibronic states in the three electronic states, and T is the diagonal free-evolution matrix whose diagonal elements are $T_{jj} = e^{-iE_j\Delta t/\hbar}$, where E_j is the eigenenergy of the jth state labeled with an index $j = \{\alpha v K m\}$, representing all the quantum numbers specifying the jth state, where α denotes any of the $X\,^2\Sigma_g^+$, $A\,^2\Pi_u$, and $B\,^2\Sigma_u^+$ states of N_2^+, v is the vibrational quantum number, K is the quantum number of the total angular momentum excluding the spin angular momentum, and m is the projection of the total angular momentum on the space-fixed z axis. The pump-probe process expressed by Eq. (5) shows that the following three processes occur in a sequential manner: (i) the excitation of N_2^+ by a strong half-Gaussian laser pulse whose peak intensity is 6×10^{14} W/cm^2, (ii) the field-free evolution, and (iii) the excitation by a weaker probe pulse whose peak intensity is 3×10^{14} W/cm^2.

Each column of the S matrix is a solution of the time-dependent Schrödinger equation obtained when N_2^+, prepared in a rovibronic state at $t = 0$, interacts with the laser pulse until the pulse vanishes. (For more details of the simulation see the Appendix.) For example, the final state $\Psi_S(\mathbf{r}, t = t_{\text{final}})$ obtained after the excitation of N_2^+ in an initial state represented as $\psi_{\alpha v K m}(\mathbf{r})$ at $t = 0$,

$$\Psi_S(\mathbf{r}, t = 0) = \psi_{\alpha v K m}(\mathbf{r}), \tag{6}$$

is given by

$$\Psi_S(\mathbf{r}, t = t_{\text{final}}) = \sum_{\alpha'} \sum_{v'} \sum_{K'} \sum_{m'=-K'}^{K'} C_{\alpha' v' K' m'} \psi_{\alpha' v' K' m'}(\mathbf{r}), \tag{7}$$

where t_{final} is set equal to $2\tau_{\text{FWHM}}$. The S-matrix elements defined as

$$S_{\alpha' v' K' m', X \alpha v K m} = C_{\alpha' v' K' m'} \tag{8}$$

can be interpreted as the coefficient of the $\psi_{\alpha' v' K' m'}(\mathbf{r})$ after N_2^+ is excited through the interaction with a given electric field from the initial state whose wave function is $\psi_{\alpha v K m}(\mathbf{r})$. When $\alpha' = \alpha$, the S matrix $S_{\alpha\alpha}$ represents the amplitude of an α-β-α type of transition, in which α is vibrationally excited or deexcited through the interaction with β. Hereafter, we call this type of excitation a Raman-type transition.

In order to simulate the intensity of the transitions from rovibrational states in the $B(0)$ state to those in the $X(0)$ states, we assume that the gain G of the lasing is represented as

$$G = e^{gL}, \tag{9}$$

where L is the length of the column in which light is amplified. The gain coefficient g in Eq. (9) is defined as

$$g = \Delta P \rho \sigma, \tag{10}$$

where ΔP represents the population difference between the two rovibronic states, ρ is the density of N_2^+, and σ is the cross section for stimulated emission. Because it can be assumed that the three parameters L, ρ, and σ do not vary in the lasing process, the logarithm of the gain given by

$$\ln(G) = \Delta P(L \rho \sigma) \tag{11}$$

indicates that the logarithm of the time-dependent emission spectrum is proportional to the population difference at a given delay time.

The rotational transition selection rule for the $B\,^2\Sigma_u^+$-$X\,^2\Sigma_g^+$ transition is $\Delta K = \pm 1$. Therefore, the $B(0)$-$X(0)$ emission spectrum of N_2^+ at 391 nm is composed of the P-branch and R-branch transitions. An excess of the population in the upper rotational level in the $B(0)$ state with respect to that in the lower rotational level in the $X(0)$ state is given by

$$\Delta P_{(K,K+1)} = P_{B,v=0,K} - P_{X,v=0,K+1} \tag{12}$$

for the P-branch emission transition and by

$$\Delta P_{(K+1,K)} = P_{B,v=0,K+1} - P_{X,v=0,K} \tag{13}$$

for the R-branch emission transition.

B. Simulation of temporal evolution of the *B*-*X* emission spectrum

We solve the time-dependent Schrödinger equation with a sufficiently small time step (1 a.u.) to derive the time-dependent population dynamics in the three lowest-energy electronic states of N_2^+, that is, the $X\,^2\Sigma_g^+$ state, the doubly degenerate $A\,^2\Pi_u$ state composed of the A_+ state and the A_- state, and the $B\,^2\Sigma_u^+$ state, as a function of the pump-probe delay time [4,25]. In each electronic state, the four lowest-lying vibrational states ($v = 0$, 1, 2, and 3) are included in the calculation, and in each vibrational state, the highest rotational quantum number is set as $K_{\max} = 40$. The initial populations in the rotational levels at $t = 0$ are assumed to be given by the Boltzmann distribution at room temperature ($T = 300$ K). The potential energy curves of the electronic states are assumed to be represented by a Morse potential given by

$$V_{\alpha'}(r) = T_{e\alpha'} + D_{e\alpha'}(e^{-\alpha_{\alpha'}(r - r_{e\alpha'})} - 1)^2, \tag{14}$$

whose parameters are taken from Ref. [20]. We calculate the coupling strengths between the rovibronic states using the transition dipole moments for the A-X and B-X transitions given by Refs. [33,34].

In the simulation, the laser field parameters are set to be the same as those in the experiment. Because the pulse durations (FWHM) of the linearly polarized near-IR (800-nm) pump and probe pulses whose polarization directions are parallel to each other are set equal to 7 fs, their spectral bandwidths (approximately 135 nm) are sufficiently large to cover the $A(0)$-$X(0)$ transition at 1108 nm. The envelope functions of the pump and probe pulses are those defined in Sec. III A. The peak intensity I_0 of the pump pulse is 6×10^{14} W cm^{-2} and that of the probe pulse is 3×10^{14} W cm^{-2}. The pump-probe delay time Δt is set to be in the range of 40–500 fs. The minimum value of Δt is set to be 40 fs so that the temporal overlap of pump and probe pulses is avoided.

Upon the creation of N_2^+ at $t = 0$, the relative probabilities of the tunneling ionization of N_2 to the $X\,^2\Sigma_g^+$, $A\,^2\Pi_u$, and the $B\,^2\Sigma_u^+$ states of N_2^+ at a laser field intensity of 6×10^{14} W cm^{-2} are estimated by the Ammosov-Delone-Krainov formula [35] to be 71.31%, 11.81%, and 16.88%, respectively. Because the Franck-Condon factor of the ionization from the vibrational ground state of the electronic ground state of neutral N_2 to the vibrational ground state of the $X\,^2\Sigma_g^+$ state [the $X(0)$ state] of N_2^+ is calculated to be 0.9, it is assumed in the simulation for simplicity that N_2^+ generated by the irradiation of an intense pump laser pulse is prepared exclusively in the $X(0)$ level at $t = 0$. A rotational wave packet created through the ionization process is calculated using the angle-dependent ionization rate in a procedure described in Appendix A.

The B-X emission spectrum shown in Fig. 2(b) is given by a weighted sum of the intensities of the respective rovibronic emission transitions as

$$I(\lambda, t) \sim \sum_{K',K''} \frac{1}{\tau\sqrt{2\pi}} \exp\left(-\frac{(\lambda - \lambda_{K',K''})^2}{2\tau^2}\right) \Delta P_{(K',K'')}, \tag{15}$$

where τ, representing the spectral resolution, is $\tau = 0.2$ nm, $\lambda_{K',K''}$ is the wavelength of the emission transition from the rotational level of $B(0)$ to the rotational level of $X(0)$, and the

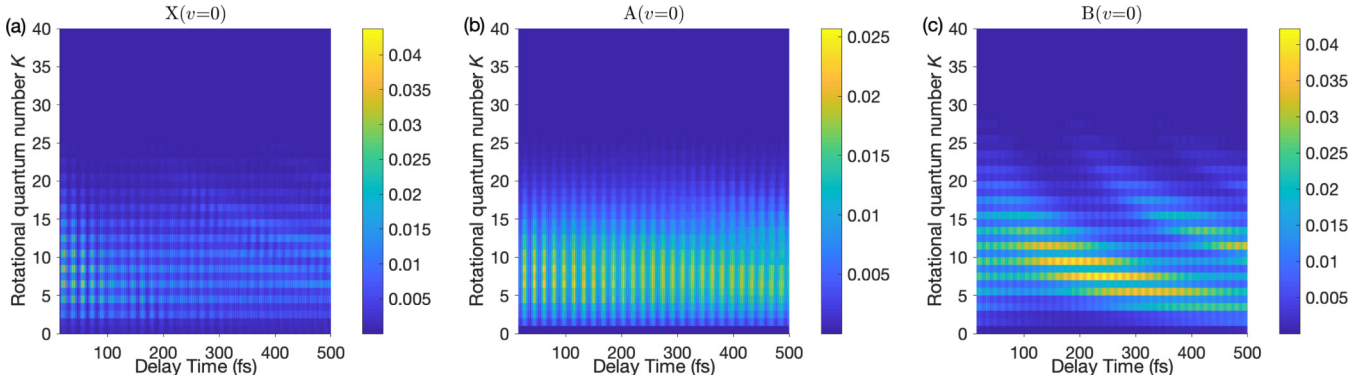

FIG. 3. Rotational population distributions in the (a) $X\,^2\Sigma_g{}^+(v=0)$, (b) $A\,^2\Pi_u(v=0)$, and (c) $B\,^2\Sigma_u{}^+(v=0)$ states of $N_2{}^+$ as a function of the pump-probe delay time

population excess $\Delta P_{(K',K'')}$ is defined as

$$\Delta P_{(K',K'')} = P^f_{B,v=0,K'} - P^f_{X,v=0,K''}, \tag{16}$$

where $P^f_{\alpha v j}$ is the final population after the interaction with the pump and probe pulses. According to the selection rule of the B-X rotational transitions, $K' = K'' \pm 1$ holds.

In the calculated emission spectrum shown in Fig. 2(b), the characteristic temporal evolutions of the intensity profiles appearing in the experimental spectrum [Fig. 2(a)] are reproduced well, that is, the P-branch transitions whose peak position in the spectrum does not change in the entire delay time range and the R-branch transitions exhibit the two ridge lines $R1$ and $R2$ whose peak positions shift towards the longer-wavelength side as the pump-probe delay time increases. The appearance of the two R-branch profiles can be ascribed to the temporal variation of the population differences between the rotational levels in the $X(0)$ state and those in the $B(0)$ state, as will be described in Sec. III C. Furthermore, the fine oscillation, corresponding to the vibrational level separations in the respective electronic states, with a period of 13–20 fs appearing in the experimental spectrum [Fig. 2(a)], is also reproduced well in the calculated emission spectrum [Fig. 2(b)].

C. Temporal variation of the population in the rovibronic levels of $N_2{}^+$

In order to clarify how the populations are transferred in the time domain among the rotational levels in the three vibronic states $B(0)$, $A(0)$, and $X(0)$ involved in the air lasing, we calculate the delay-time-dependent populations in the respective rotational levels. Among the four vibrational states of the $A\,^2\Pi_u$ state included in the simulation, we examine the case in which the $A(0)$ state is involved because the Franck-Condon factor of the excitation from the $X(0)$ state to the $A(0)$ state whose value is 0.49 is larger than 0.32 for the $A(1)$ state, 0.13 for the $A(2)$ state, and 0.04 for $A(3)$ state. The results of the simulation are shown in Fig. 3 represented as a function of the pump-probe delay time. The population distributions in the rotational levels in the $B(0)$ state exhibit a tilted stripe pattern. At $\Delta t = 100$ fs, the population maximum is located at $K = 10$, and the maximum position moves towards the lower K as the delay time increases. At $\Delta t = 250$ fs, two population maxima are located at $K = 10$ and 22. As Δt increases, this second population maximum at $K = 22$ at $\Delta t = 250$ fs moves towards the lower K. At $\Delta t = 450$ fs, three population maxima appear in the rotational distributions. This type of characteristic oscillation of the populations in the respective rotational levels can only vaguely be seen in the $X(0)$ state and can scarcely be seen in the $A(0)$ state. The markedly different rotational distributions in these three vibronic states can be ascribed to the creation of a rotational wave packet in the $B(0)$ state through the coherent population transfer among the rotational levels by Raman-type transitions, i.e., the $B(0)$-$X(0)$-$B(0)$ type of transitions, induced by the probe pulse through the $X(v)$ state.

As described above in Sec. III A, the populations in the respective rovibronic levels in the final state of $N_2{}^+$ after the interaction with a sudden turn-on pump pulse followed by the interaction with a weaker probe pulse at certain delay time can be given by Eq. (5). In the simulation, we neglect the rotational excitation within the neutral manifold because the effect of the rotational excitation of neutral N_2 induced by the pump pulse before the ionization on the final population distribution of $N_2{}^+$ is negligibly small [26]. The final population in a rotational level specified by a set of quantum numbers (K', m) in the $B(0)$ state at time $t = \Delta t + 2\tau_{\rm FWHM}$ is given by

$$P_{BK'm}(t) = \sum_{K''=0}^{K_{\max}} C^X_{K''m} \left| c^{XK''m}_{BK'm}(t) \right|^2, \tag{17}$$

where $C^X_{K''m}$ is the population in the $|X0K''m\rangle$ level at $t = 0$ given by the Boltzmann distribution at 300 K, which can be expressed as

$$C^X_{K''Xm} = \frac{1}{\zeta} g_{K''} e^{-B_X K''(K''+1)/k_B T} \tag{18}$$

using the Boltzmann factor given in the Appendix, and $|c^{X0K''m}_{B0K'm}(t)|^2$ is the final population transferred from the $|X0K''m\rangle$ level to the $|B0K'm\rangle$ level.

Because m is conserved throughout the pump-probe process, m is omitted in the equations below. In addition, because only the transitions among the vibrational ground states of the three electronic states are examined below, a vibrational quantum number of 0 specifying the vibrational ground states is omitted in the equations hereafter. With the simplified

notation, Eq. (17) can be written as

$$P_{BK'}(t) = \sum_{K''=0}^{K_{\max}} C_{K''}^{X} \left| c_{BK'}^{XK''}(t) \right|^2, \tag{19}$$

using the coefficient $c_{BK'}^{XK''}(t)$ given by

$$c_{BK'}^{XK''}(t) = \sum_{\alpha} \sum_{v} \sum_{K} S_{BK'\alpha K}^{\text{probe}} S_{\alpha K X K''}^{\text{pump}} e^{-iE_{\alpha v K} t_f/\hbar}, \tag{20}$$

where the S-matrix element $S_{\alpha K X K''}^{\text{pump}}$ stands for the population transfer from $|X0K''\rangle$ to $|\alpha 0K\rangle$ by the pump pulse, the S-matrix element $S_{BK'\alpha K}^{\text{probe}}$ stands for the population transfer from $|\alpha 0K\rangle$ to $|B0K''\rangle$ by the probe pulse, and t_f is the free-evolution time between the pump and probe pulses defined as $t_f = \Delta t - 4\tau_{\text{FWHM}}$, which ensures that the pump pulse vanishes by the time the probe pulse starts interacting with N_2^+.

The populations in the rotational levels in the $B(0)$ state are created by the near-IR sudden turn-on pump pulse and modified by the Raman-type rotational transitions within the $B(0)$ state induced by both the pump and probe pulses. The population in the $|X0K''\rangle$ level is mainly transferred to the $|B0K'' \pm 1\rangle$ level by the pump-pulse S matrix. Indeed, the numerical value of the squared modulus of the S-matrix element for the $\Delta K = +1$ transition from $K'' = 0$ and $m = 0$ is $|S_{B(K=1)X0}^{\text{pump}}|^2 = 0.12$, while the magnitude of the S-matrix element of the $\Delta K \geqslant 2$ transitions from $K'' = 0$ and $m = 0$ are all very small, that is, $|S_{B(K\neq 1)X0}^{\text{pump}}|^2 < 10^{-4}$. This means that the population transfer to the $B(0)$ state is achieved by a one-photon transition induced by the weak tail component of the spectrum of the sudden turn-on pump pulse extending to the higher-frequency domain. When we consider the transition from the $|X0(K' = 0)\rangle$ level, m is 0 by definition. The same analysis is performed for $m > 0$ and $K' > 0$ and all the contributions from the different m values are added, as will be shown in Eq. (22).

On the other hand, the values of the squared modulus of the S-matrix element for the probe pulse $|S_{BK'B0}^{\text{probe}}|^2$ are 0.08 for $K' = 0$, 0.52 for $K' = \pm 2$, 0.30 for $K' = \pm 4$, and 0.06 for $K' = \pm 6$, showing that a $|B0K\rangle$ level is coupled with a $|B0K'\rangle$ level with $K' = K \pm 2, K \pm 4, K \pm 6 \ldots$, through the sequential Raman-type transitions. Consequently, Eq. (17) can be expressed approximately as

$$P_{BK'}(t) = \sum_{K''-K=\pm 1} C_{K''}^{X} \times \left| \sum_{K-K'=\pm 2,\pm 4} S_{BK'BK}^{\text{probe}} S_{BKXK''}^{\text{pump}} e^{-iE_{BK} t_f/\hbar} \right|^2. \tag{21}$$

It is found from the numerical analysis that the temporal variation of the population $P_{BK'}(t)$ is governed by the real part of the terms $e^{-i(E_{B(K'\pm 4)} - E_{B(K'\pm 2)})t_f/\hbar}$. The real part oscillating in time shows that the period becomes shorter as the rotational quantum number K' increases. As shown in Fig. 3(c), the period of the oscillation of the population in the rotational levels in the $B(0)$ states decreases from 400 fs to 200 fs as K' increases from 11 to 25.

The temporal evolution of the population in the rotational levels in the $X(0)$ states is much less pronounced compared with that in the $B(0)$ states. Therefore, the emission spectrum, reflecting the difference in the population in the rotational levels in the $B(0)$ state and the population in the rotational levels in the $X(0)$ state, exhibits the oscillation originating mainly from the temporal evolution of the population in the $B(0)$ state, resulting in the appearance of the two ridges in the temporal evolution of the R-branch transition intensities. By comparing the emission spectrum shown in Fig. 2(b) and the population distribution in Fig. 3(c), it can be seen that the $R2$ branch in Fig. 2(b) starts around 300 fs and the signal becomes stronger as the delay time increases, corresponding to the second tilted distribution in the stripe pattern in Fig. 3(c), where the highly excited rotational levels have a small amount of population around 300 fs, and as the delay time increases, the populations in the lower rotational levels in the $B(0)$ state increases. The $R1$ and $R2$ ridges appearing in Fig. 2(b) correspond respectively to the first and second tilted pattern in the stripe pattern appearing in Fig. 3(c), reflecting the temporal evolution of the population in the rotational levels of the $B(0)$ state.

In order to examine how the rotational excitations are achieved in the $X(0)$, $A(0)$, and $B(0)$ states by the pump and probe pulses, we show in Fig. 4 the populations in the rotational levels in the $X(0)$, $A(0)$, and $B(0)$ states at three different times, i.e., (i) just after the ionization at $t = 0$ fs, (ii) just after the interaction with the pump pulse $t = 14$ fs, and (iii) after the interaction with the probe pulse at $t = (350 + 14)$ fs.

The zigzag patterns appearing in the K dependence of the populations seen in Fig. 4(a) for the $X(0)$, $A(0)$, and $B(0)$ state are ascribed to the nuclear spin statistical weights of N_2^+ (see the Appendix), that is, $g_K = 2$ for the rotational levels with even K and $g_K = 1$ for the rotational levels with odd K. As shown in Fig. 4(c), because the selection rule of the $B\,^2\Sigma_u^+$-$X\,^2\Sigma_g^+$ transition is $\Delta K = \pm 1$, the phase of the zigzag pattern appearing in the population distribution in the $B(0)$ state is inverted with respect to that in the $X(0)$ state. Interestingly, as shown in Fig. 4(b), the zigzag pattern is much less pronounced in the population distribution in the $A(0)$ state. This suppression of the zigzag pattern can be interpreted by the fact that the doubly degenerate $A\,^2\Pi_u$ state is composed of the two degenerate states, that is, the A_+ state and the A_- state. The rotational selection rule of the A_--X transition is $\Delta K = \pm 1$, generating a zigzag pattern of the A_- state similar to that of the B state, while the rotational selection rules of the A_+-X transition is $\Delta K = 0$, generating a zigzag pattern of the A_+ state similar to that of the X state. Because these two zigzag patterns are out of phase with each other, the zigzag pattern appearing in the sum of the population distribution of A_- state and A_+ state becomes unclear, as shown in Fig. 4(b).

In order to understand the origin of the difference between the extent of the rotational excitation achieved in the $B(0)$ state and that achieved in the $A(0)$ state induced by a full-Gaussian shape probe pulse, the S-matrix elements representing the transition probabilities between the rovibronic levels are examined. As shown in Fig. 5, the transition probabilities of the Raman-type X-(A or B)-X, A-X-A, and B-X-B transitions induced by the probe pulse are plotted as a function of the rotational quantum number K for the $X\,^2\Sigma_g^+$, $A\,^2\Pi_u$, and $B\,^2\Sigma_u^+$ states, respectively. The transition probabilities are obtained from the S matrix representing the excitation achieved by the probe pulse, that is, the transition probability

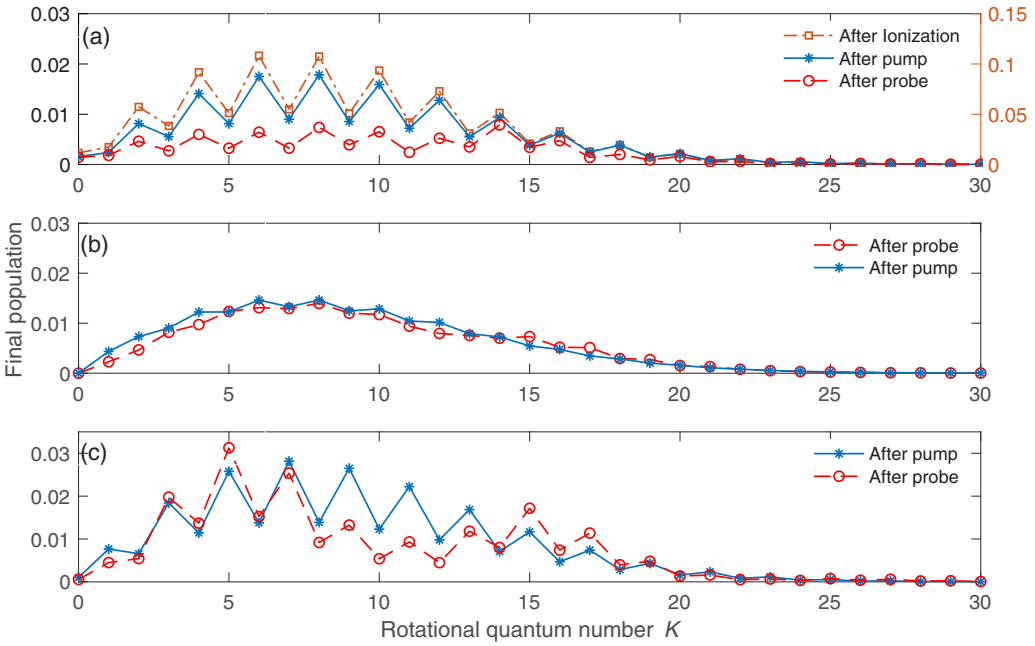

FIG. 4. Rotational population distributions in the (a) $X\,^2\Sigma_g{}^+(v=0)$, (b) $A\,^2\Pi_u(v=0)$, and (c) $B\,^2\Sigma_u{}^+(v=0)$ states of $N_2{}^+$ just after the ionization [only for (a) with the vertical axis on the right side], just after the pump pulse, and after the probe pulse at a delay time of 350 fs. Because it is assumed that $N_2{}^+$ is prepared exclusively in the $X\,^2\Sigma_g{}^+$ state after ionization, no "after ionization" line is shown in (b) or (c).

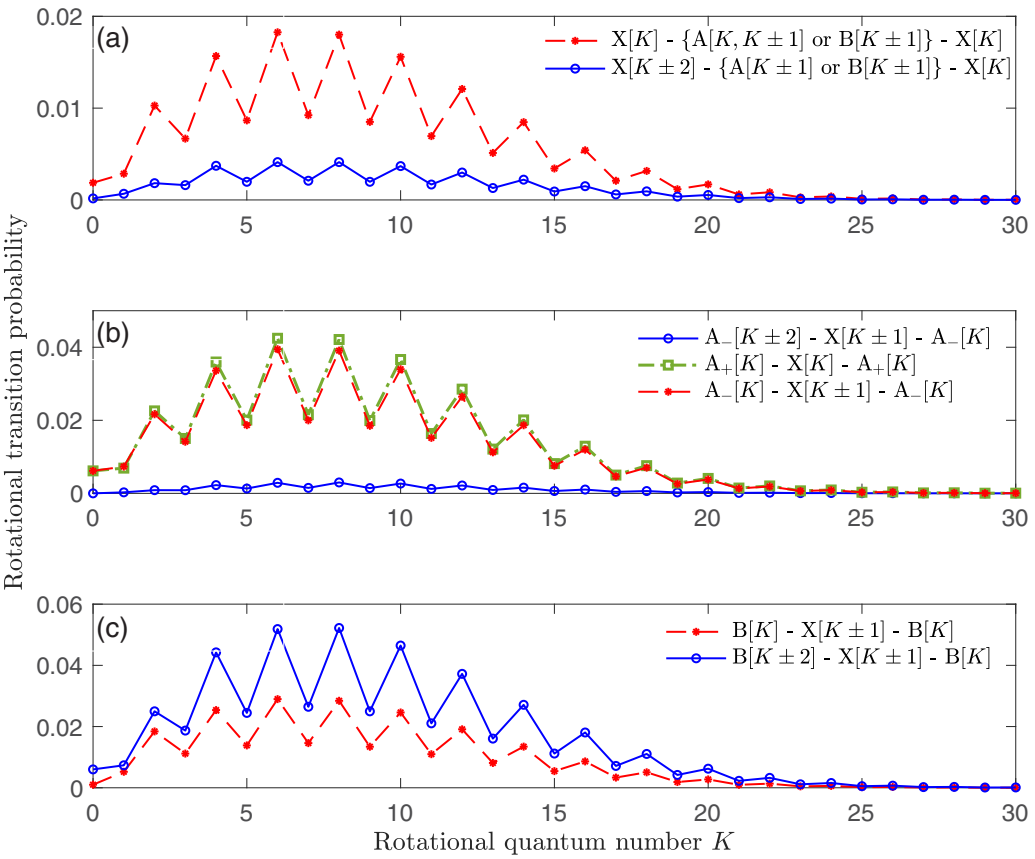

FIG. 5. Rotational transition probabilities in the (a) $X\,^2\Sigma_g{}^+(0)$, (b) $A\,^2\Pi_u(0)$, and (c) $X\,^2\Sigma_g{}^+(0)$ states of $N_2{}^+$ by the probe pulse through the Raman-type transitions. The red dotted zigzag lines represent the probabilities for the population to remain in the same rotational level and the blue zigzag lines show the probabilities for the population to be transferred to the other rotational levels.

for the Raman-type $|\alpha v_\alpha K_\alpha\rangle$-$|\beta v_\beta K_\beta\rangle$-$|\alpha v_\alpha K'_\alpha\rangle$ transition is proportional to the S-matrix elements,

$$p_{|\alpha v_\alpha K_\alpha\rangle-|\beta v_\beta K_\beta\rangle-|\alpha v_\alpha K'_\alpha\rangle} \propto \sum_m C^\alpha_{K_\alpha m}\left|S^{\text{probe}}_{\alpha v_\alpha K_\alpha m,\alpha v_\alpha K'_\alpha m}\right|^2, \quad (22)$$

where $C^\alpha_{K_\alpha m}$ is the Boltzmann coefficient for the $|K_\alpha, m\rangle$ level in the $X\,^2\Sigma_g{}^+$ state.

For the B-X-B transitions, within the framework of the second-order perturbation, there are four different Raman-type pathways, that is, the two pathways that do not change the K rotational quantum number, $B[K] \to X[K+1] \to B[K]$ and $B[K] \to X[K-1] \to B[K]$, and the two pathways that change the K rotational quantum number by 2, $B[K+2] \to X[K+1] \to B[K]$ and $B[K-2] \to X[K-1] \to B[K]$, corresponding to the rotational deexcitation and excitation, respectively. For the A-X-A transition, within the framework of the second-order perturbation, there are five different Raman-type pathways, that is, the three pathways that do not change the K rotational quantum number, $A[K] \to X[K] \to A[K]$, $A[K] \to X[K+1] \to A[K]$, and $A[K] \to X[K-1] \to A[K]$, and the two pathways that change the K rotational quantum number by 2, $A[K+2] \to X[K+1] \to A[K]$ and $A[K-2] \to X[K-1] \to A[K]$, corresponding to the rotational deexcitation and excitation, respectively.

The significant difference between the A-X-A transition and the B-X-B transition comes from the difference between the rotational selection rules and the difference between the transition probabilities of the $X\,^2\Sigma_g{}^+$-$B\,^2\Sigma_u{}^+$ transition and those of the $X\,^2\Sigma_g{}^+$-$A\,^2\Pi_u$ transition. First, only the A-X-A transition has a route with $\Delta K = 0$, that is, the $A[K] \to X[K] \to A[K]$ transition, represented as the green dash-dotted zigzag line in Fig. 5(b). Second, as has already been examined in [26], the $X[K] - A[K+1]$ transition has stronger intensity than the $X[K] - A[K-1]$ transition, while the $X[K] - B[K+1]$ transition has the same strength as the $X[K] - B[K-1]$ transition, resulting in the marked difference in the relative transition intensities between the red dashed zigzag line and the blue solid zigzag line in Fig. 5(b).

The red dashed zigzag line in Fig. 5 shows the probability for the population in each rotational level to remain in the same rotational level and the blue zigzag line shows the probability for the population to be transferred to the higher and lower rotational levels after the interaction with the probe pulse. The comparison between the red dotted zigzag line and blue solid zigzag line in Fig. 5(c) for the B-X-B transition shows that the probability of the population remaining in the initial rotational level is only about one-half of the probability of the population transferred to the other rotational level, which makes the rotational excitation and deexcitation proceed efficiently in the $B(0)$ state. On the other hand, as shown in Fig. 5(b), the red dotted zigzag line in the A-X-A transition is much larger than the blue solid zigzag line in Fig. 5(b), which means that the population in the rotational levels in the $A\,^2\Pi_u$ state almost remain in the initial rotational state and that the rotational excitation and deexcitation in the $A(0)$ state are not pronounced efficiently.

Because the $X\,^2\Sigma_g{}^+$ state is shared by the $A\,^2\Pi_u$-$X\,^2\Sigma_g{}^+$ transition and the $B\,^2\Sigma_u{}^+$-$X\,^2\Sigma_g{}^+$ transition, the population in the rotational levels of $X(0)$ state after the interaction with the probe pulse is influenced by both the X-B-X and X-A-X couplings. As shown in Fig. 5(a), the probability of the population transfer with $\Delta K = 0$, represented by the red dotted zigzag line, is several times larger than that with $\Delta K = K \pm 2$ represented by the blue solid zigzag line, which shows that the extent of the rotational excitation in the X state becomes intermediate between that in the $B(0)$ state and that in the $A(0)$ state.

IV. CONCLUSION

The coherent lasing at 391 nm corresponding to the P-branch and R-branch transitions of the $B\,^2\Sigma_u{}^+(v=0)$-$X\,^2\Sigma_g{}^+(v=0)$ emission were generated and recorded by irradiating N_2 gas with a sequential linearly polarized intense pump and probe pulses. In the temporal evolution of the emission spectrum, the R branch exhibits two ridges $R1$ and $R2$ and the most intense peak in the R-branch emission shifts from the higher-frequency region to the low-frequency region.

By applying the time-dependent rovibronic model that we introduced to simulate the population transfer induced by a pump intense laser field after the ionization [26], we showed that the theoretically obtained temporal evolution of the intensity distributions in the P-branch and R-branch structures of the $B\,^2\Sigma_u{}^+$-$X\,^2\Sigma_g{}^+$ emission, reflecting the population difference between the $X(0)$ and $B(0)$ states, is in good agreement with the experimental observation.

While the populations in the respective rotational levels of the $B(0)$ state show a periodic time dependence, the temporal variation in the population distribution of $X(0)$ is less pronounced, which results in the creation of the two ridges in the R-branch emissions, reflecting the difference between the temporal evolution of the population distribution in the $X(0)$ state and that in the $B(0)$ state. We interpreted the difference in the temporal evolutions as the difference in the coupling strength and that in the selection rules in the $B\,^2\Sigma_u{}^+$-$X\,^2\Sigma_g{}^+$ transition and $A\,^2\Pi_u$-$X\,^2\Sigma_g{}^+$ transition. We revealed that the characteristic temporal evolution of the rotational structure in the emission spectrum of air lasing at 391 nm can be realized by the different rotational selection rules of the electronic transitions involved in the rotational population transfer processes.

ACKNOWLEDGMENTS

This research was supported by JSPS KAKENHI Grants No. 15K17805, No. 15H05696, and No. 20H00371, and by NSFC (61625501) Grant from National Natural Science Foundation of China.

APPENDIX: TIME-DEPENDENT ROVIBRONIC DYNAMICS OF $N_2{}^+$ IN AN INTENSE LASER FIELD

The time-dependent dynamics of $N_2{}^+$ interacting with a light field can be described by the time-dependent Schrödinger equation

$$i\hbar\frac{\partial}{\partial t}\Psi(\mathbf{r},t) = H(t)\Psi(\mathbf{r},t), \quad (A1)$$

where $H(t)$ is the Hamiltonian operator

$$H(t) = -\frac{\hbar^2}{2m_\mu}\nabla^2 + V(\mathbf{r}) + H_1(t), \quad (A2)$$

m_μ is the reduced mass of $N_2{}^+$, $V(\mathbf{r})$ is the interatomic potential energy curve represented as a function of the internuclear distance $\mathbf{r}$, and $H_1(t) = \vec{\mu} \cdot \vec{\mathcal{E}}(t)$ stands for the light-molecule interaction with the linearly polarized electric field expressed as $\vec{\mathcal{E}}(t)$, whose polarization direction is along the space-fixed z axis. The time-dependent wave function of the rovibrational levels in the $X\,^2\Sigma_g{}^+$, $A\,^2\Pi_u$, and $B\,^2\Sigma_u{}^+$ states of $N_2{}^+$ can be expressed as

$$\Psi(\mathbf{r}, t) = \sum_\alpha \sum_v \sum_K \sum_{m=-K}^{K} c_{\alpha v K m}(t)\psi_{\alpha v K m}(\mathbf{r}). \tag{A3}$$

Here α denotes any of the $X\,^2\Sigma_g{}^+$, $A\,^2\Pi_u$, and $B\,^2\Sigma_u{}^+$ states of $N_2{}^+$, v is the vibrational quantum number, K is the quantum number of the total angular momentum excluding the spin angular momentum, m is the projection of the total angular momentum excluding the spin angular momentum onto the space-fixed z axis, and $\mathbf{r}$ is the internuclear distance vector whose absolute value is r. The basis wave function of the Kth rotational state in the vth vibrational state in the electronic state α, denoted by $\psi_{\alpha v K m}(\mathbf{r})$, is represented as a product of the electronic, vibrational, and rotational basis sets as [26]

$$\psi_{\alpha v K m}(\mathbf{r}) = |\alpha\rangle\, |v\rangle^{\alpha, K}\, |K, m\rangle^{\alpha}\,, \tag{A4}$$

where $|\alpha\rangle$ is the electronic wave function, $|v\rangle^{\alpha,K}$ is the vibrational basis wave function obtained as the solution of the one-dimensional time-independent Schrödinger equation with the Morse potential (14), and the rotational basis function $|K, m\rangle^{\alpha}$ is defined as

$$|K, m\rangle^{\alpha} = \begin{cases} |K, m, 0\rangle & \text{when } \alpha = X \text{ or } B \\ (|K, m, 1\rangle + |K, m, -1\rangle)/\sqrt{2} & \text{when } \alpha = A_+ \\ (|K, m, 1\rangle - |K, m, -1\rangle)/\sqrt{2} & \text{when } \alpha = A_-. \end{cases} \tag{A5}$$

This equation was introduced in [26], but the coefficient 2 appearing in the corresponding equation, Eq. (6) in [26], should be replaced by $\sqrt{2}$. In Eq. (A5), the rotational wave functions $|K, m, k\rangle$ are defined as [36]

$$|K, m, k\rangle = \frac{1}{\sqrt{2}}\sqrt{(K+m)!(K-m)!(K+k)!(K-k)!(2K+1)}\sum_\sigma (-1)^\sigma \frac{[\cos(\theta/2)]^{2K+k-m-2\sigma}[-\sin(\theta/2)]^{m-k+2\sigma}}{\sigma!(K-m-\sigma)!(m-k+\sigma)!(K+k-\sigma)!}e^{im\phi}, \tag{A6}$$

where θ is the polar angle, ϕ is the azimuth angle, and k is the projection of electronic orbital angular momentum on the molecular axis connecting two nitrogen nuclei. These wave functions can also be expressed in Wigner D functions [37]. For the $X\,^2\Sigma_g{}^+$ and $B\,^2\Sigma_u{}^+$ states, the projection k is $k = 0$, and $|K, m, 0\rangle$ becomes a spherical harmonic function. For the doubly degenerate $A\,^2\Pi_u$ state, with $k = \pm 1$, the two basis functions $|K, m\rangle^{A_+}$ and $|K, m\rangle^{A_-}$, given by Eq. (A5), are symmetric with respect to the transformation $\theta \to \pi - \theta$, while the rotational wave functions $|K, m, +1\rangle$ and $|K, m, -1\rangle$, given by Eq. (A6), are not symmetric with respect to the transformation $\theta \to \pi - \theta$.

The transition probability between rotational levels in the ground electronic $X\,^2\Sigma_g{}^+$ state and the rotational levels in the electronically excited $A\,^2\Pi_u$ or $B\,^2\Sigma_u{}^+$ state is given by

$$\left|p^{K,m}_{X\beta(\Delta K_\beta)}\right|^2 = |{}^X\langle K, m|F_\theta^{X\beta}|K + \Delta K_\beta, m\rangle^\beta|^2, \tag{A7}$$

where $\Delta K_B = \pm 1$ for $\beta = B$, $\Delta K_{A_\pm} = \pm 1, 0$ for $\beta = A_\pm$, and $F_\theta^{\alpha\beta}$ is the angular factor defined as [33,34,37]

$$F_\theta^{\alpha\beta} = \cos(\theta)(\delta_{B\alpha}\delta_{X\beta} + \delta_{X\alpha}\delta_{B\beta}) + \frac{\sin(\theta)}{\sqrt{2}}(\delta_{A_\pm\alpha}\delta_{X\beta} + \delta_{X\alpha}\delta_{A_\pm\beta}). \tag{A8}$$

For given K and m,

$$p^{K,m}_{XB(\Delta K_B)} = \begin{cases} \left(\frac{(K-m+1)(K+m+1)}{(2K+1)(2K+3)}\right)^{1/2} & \text{when } \Delta K_B = 1 \\ \left(\frac{(K-m)(K+m)}{(2K+1)(2K-1)}\right)^{1/2} & \text{when } \Delta K_B = -1, \end{cases} \tag{A9}$$

$$\begin{aligned} p^{K,m}_{XA_\pm(\Delta K_{A_\pm})} &= K!\sqrt{(K+m)!(K-m)!(K+\Delta K_{A_\pm}+m)!(K+\Delta K_{A_\pm}-m)!} \\ &\times \sqrt{(K+\Delta K_{A_\pm}+1)!(K+\Delta K_{A_\pm}-1)!(2K+1)[2(K+\Delta K_{A_\pm})+1]} \\ &\times \sum_{\sigma=0}^{K-m}\left\{\frac{(-1)^\sigma}{\sigma!(K-m-\sigma)!(m+\sigma)!(K-\sigma)!(2+2K+\Delta K_{A_\pm})!}\right. \\ &\times \left[\sum_{\sigma'}(-1)^{\sigma'-1}\frac{(1-m+2K+\Delta K_{A_\pm}-\sigma-\sigma')!(m+\sigma+\sigma')!}{\sigma'!(K+\Delta K_{A_\pm}-m-\sigma')!(m-1+\sigma')!(K+\Delta K_{A_\pm}+1-\sigma')!}\right. \\ &\left.\left. + (-1)^{\Delta K_{A_\pm}}\sum_{\sigma_s'}(-1)^{\sigma_s'+1}\frac{(2K-m+\Delta K_{A_\pm}-\sigma-\sigma_s')!(1+m+\sigma+\sigma_s')!}{\sigma_s'!(K+\Delta K_{A_\pm}-m-\sigma_s')!(m+1+\sigma_s')!(K+\Delta K_{A_\pm}-1-\sigma_s')!}\right]\right\}, \end{aligned} \tag{A10}$$

where σ' starts from the larger of 0 and $1-m$ and ends at $K+\Delta K_{A_\pm}-m$, and σ_s' starts from 0 and ends at the smaller of $K+\Delta K_{A_\pm}-m$ and $K+\Delta K_{A_\pm}-1$. These coupling terms can also be represented in the Wigner 3-j symbols as shown in [38].

The probability of finding the system in the rotational state with the rotational quantum numbers K in the vth vibrational state of the electronic state α is given by

$$P_{\alpha vK'}(t)=\frac{1}{\zeta}\sum_{K''=0}^{K_{\max}}\sum_{m=-K''}^{K''}\left|c_{\alpha vK'm}^{X0K''m}(t)\right|^2 \times g_{K''}e^{-B_XK''(K''+1)/k_BT}, \tag{A11}$$

where $c_{\alpha vK'm}^{X0K''m}(t)$ are the coefficients in Eq. (A3) determined as the solution of Eq. (A1) with the initial condition $c_{\alpha vK'm}^{X0K''m}(t=0)=\delta_{X\alpha}\delta_{0v}\delta_{K'K''}$, B_X is the rotational constant of the $X\,^2\Sigma_g{}^+(0)$ state, k_B is the Boltzmann constant, $g_{K''}$ is the nuclear spin statistical weight, which takes the values of $g_{K''}=2$ for even K'' and $g_{K''}=1$ for odd K'', and ζ is the normalization factor given by

$$\zeta=\sum_{K''=0}^{K_{\max}}g_K''(2K''+1)e^{-B_XK''(K''+1)/k_BT}. \tag{A12}$$

The rotational wave packet prepared by the ionization process from each initial rotational state in the $X\,^2\Sigma_g{}^+$ state can be calculated as

$$\Psi_{K,m}=\sum_{K'}\left(\langle K',m,0|\sqrt{\frac{I(\theta)}{\int I(\theta)\sin\theta d\theta}}|K,m,0\rangle\right)|K',m,0\rangle, \tag{A13}$$

where $I(\theta)$ is the θ-dependent ionization rate calculated by the Ammosov-Delone-Krainov formula [35].

[1] Q. Luo, W. Liu, and S. Chin, Lasing action in air induced by ultra-fast laser filamentation, Appl. Phys. B **76**, 337 (2003).

[2] J. Yao, B. Zeng, H. Xu, G. Li, W. Chu, J. Ni, H. Zhang, S. L. Chin, Y. Cheng, and Z. Xu, High-brightness switchable multiwavelength remote laser in air, Phys. Rev. A **84**, 051802(R) (2011).

[3] T.-J. Wang, J. Ju, J.-F. Daigle, S. Yuan, R. Li, and S. L. Chin, Self-seeded forward lasing action from a femtosecond Ti:sapphire laser filament in air, Laser Phys. Lett. **10**, 125401 (2013).

[4] H. Xu, E. Lötstedt, A. Iwasaki, and K. Yamanouchi, Sub-10-fs population inversion in $N_2{}^+$ in air lasing through multiple state coupling, Nat. Commun. **6**, 8347 (2015).

[5] J. Yao, S. Jiang, W. Chu, B. Zeng, C. Wu, R. Lu, Z. Li, H. Xie, G. Li, C. Yu, Z. Wang, H. Jiang, Q. Gong, and Y. Cheng, Population Redistribution Among Multiple Electronic States of Molecular Nitrogen Ions in Strong Laser Fields, Phys. Rev. Lett. **116**, 143007 (2016).

[6] H. Xu, E. Lötstedt, T. Ando, A. Iwasaki, and K. Yamanouchi, Alignment-dependent population inversion in $N_2{}^+$ in intense few-cycle laser fields, Phys. Rev. A **96**, 041401(R) (2017).

[7] Y. Liu, P. Ding, N. Ibrakovic, S. Bengtsson, S. Chen, R. Danylo, E. R. Simpson, E. W. Larsen, X. Zhang, Z. Fan, A. Houard, J. Mauritsson, A. L'Huillier, C. L. Arnold, S. Zhuang, V. Tikhonchuk, and A. Mysyrowicz, Unexpected Sensitivity of Nitrogen Ions Superradiant Emission on Pump Laser Wavelength and Duration, Phys. Rev. Lett. **119**, 203205 (2017).

[8] X. Zhong, Z. Miao, L. Zhang, Q. Liang, M. Lei, H. Jiang, Y. Liu, Q. Gong, and C. Wu, Vibrational and electronic excitation of ionized nitrogen molecules in intense laser fields, Phys. Rev. A **96**, 043422 (2017).

[9] L. Arissian, B. Kamer, A. Rastegari, D. M. Villeneuve, and J.-C. Diels, Transient gain from $N_2{}^+$ in light filaments, Phys. Rev. A **98**, 053438 (2018).

[10] A. Zhang, Q. Liang, M. Lei, L. Yuan, Y. Liu, Z. Fan, X. Zhang, S. Zhuang, C. Wu, Q. Gong, and H. Jiang, Coherent modulation of superradiance from nitrogen ions pumped with femtosecond pulses, Opt. Express **27**, 12638 (2019).

[11] Y. Liu, P. Ding, G. Lambert, A. Houard, V. Tikhonchuk, and A. Mysyrowicz, Recollision-Induced Superradiance of Ionized Nitrogen Molecules, Phys. Rev. Lett. **115**, 133203 (2015).

[12] V. T. Tikhonchuk, J.-F. Tremblay-Bugeaud, Y. Liu, A. Houard, and A. Mysyrowicz, Excitation of nitrogen molecular ions in a strong laser field by electron recollisions, Eur. Phys. J. D **71**, 292 (2017).

[13] G. Li, C. Jing, B. Zeng, H. Xie, J. Yao, W. Chu, J. Ni, H. Zhang, H. Xu, Y. Cheng, and Z. Xu, Signature of superradiance from a nitrogen-gas plasma channel produced by strong-field ionization, Phys. Rev. A **89**, 033833 (2014).

[14] X. Zhong, Z. Miao, L. Zhang, H. Jiang, Y. Liu, Q. Gong, and C. Wu, Optimizing the 391-nm lasing intensity from ionized nitrogen molecules in 800-nm femtosecond laser fields, Phys. Rev. A **97**, 033409 (2018).

[15] M. Lei, C. Wu, A. Zhang, Q. Gong, and H. Jiang, Population inversion in the rotational levels of the superradiant $N_2{}^+$ pumped by femtosecond laser pulses, Opt. Express **25**, 4535 (2017).

[16] A. Azarm, P. Corkum, and P. Polynkin, Optical gain in rotationally excited nitrogen molecular ions, Phys. Rev. A **96**, 051401(R) (2017).

[17] M. Britton, P. Laferrière, D. H. Ko, Z. Li, F. Kong, G. Brown, A. Naumov, C. Zhang, L. Arissian, and P. B. Corkum, Testing the Role of Recollision in $N_2{}^+$ Air Lasing, Phys. Rev. Lett. **120**, 133208 (2018).

[18] A. Mysyrowicz, R. Danylo, A. Houard, V. Tikhonchuk, X. Zhang, Z. Fan, Q. Liang, S. Zhuang, L. Yuan, and Y. Liu, Lasing without population inversion in $N_2{}^+$, APL Photon. **4**, 110807 (2019).

[19] M. Richter, M. Lytova, F. Morales, S. Haessler, O. Smirnova, M. Spanner, and M. Ivanov, Rotational quantum beat lasing without inversion, Optica **7**, 586 (2020).

[20] NIST Chemistry WebBook, NIST Standard Reference Database Number 69, edited by P. J. Linstrom and W. G. Mallard, available at https://doi.org/10.18434/T4D303 (National Institute of Standards and Technology, Gaithersburg, 2020).

[21] H. Li, M. Hou, H. Zang, Y. Fu, E. Lötstedt, T. Ando, A. Iwasaki, K. Yamanouchi, and H. Xu, Significant Enhance-

ment of N_2^+ Lasing by Polarization-Modulated Ultrashort Laser Pulses, Phys. Rev. Lett. **122**, 013202 (2019).

[22] T. Ando, E. Lötstedt, A. Iwasaki, H. Li, Y. Fu, S. Wang, H. Xu, and K. Yamanouchi, Rotational, Vibrational, and Electronic Modulations in N_2^+ Lasing at 391 nm: Evidence of Coherent $B^2\Sigma_u^+ - X^2\Sigma_g^+ - A^2\Pi_u$ Coupling, Phys. Rev. Lett. **123**, 203201 (2019).

[23] H. Li, E. Lötstedt, H. Li, Y. Zhou, N. Dong, L. Deng, P. Lu, T. Ando, A. Iwasaki, Y. Fu, S. Wang, J. Wu, K. Yamanouchi, and H. Xu, Giant Enhancement of Air Lasing by Complete Population Inversion in N_2^+, Phys. Rev. Lett. **125**, 053201 (2020).

[24] Y. Zhang, E. Lötstedt, and K. Yamanouchi, Population inversion in a strongly driven two-level system at far-off resonance, J. Phys. B **50**, 185603 (2017).

[25] Y. Zhang, E. Lötstedt, and K. Yamanouchi, Mechanism of population inversion in laser-driven N_2^+, J. Phys. B **52**, 055401 (2019).

[26] Y. Zhang, E. Lötstedt, and K. Yamanouchi, Rotationally induced population inversion between the $B^2\Sigma_u^+$ and $X^2\Sigma_g^+$ states of N_2^+ exposed to an intense laser pulse, Phys. Rev. A **101**, 053412 (2020).

[27] H. Xie, H. Lei, G. Li, Q. Zhang, X. Wang, J. Zhao, Z. Chen, J. Yao, Y. Cheng, and Z. Zhao, Role of rotational coherence in femtosecond-pulse-driven nitrogen ion lasing, Phys. Rev. Res. **2**, 023329 (2020).

[28] H. Zhang, C. Jing, J. Yao, G. Li, B. Zeng, W. Chu, J. Ni, H. Xie, H. Xu, S. L. Chin, K. Yamanouchi, Y. Cheng, and Z. Xu, Rotational Coherence Encoded in an "Air-Laser" Spectrum of Nitrogen Molecular Ions in an Intense Laser Field, Phys. Rev. X **3**, 041009 (2013).

[29] B. Zeng, W. Chu, G. Li, J. Yao, H. Zhang, J. Ni, C. Jing, H. Xie, and Y. Cheng, Real-time observation of dynamics in rotational molecular wave packets by use of air-laser spectroscopy, Phys. Rev. A **89**, 042508 (2014).

[30] H. Xie, B. Zeng, G. Li, W. Chu, H. Zhang, C. Jing, J. Yao, J. Ni, Z. Wang, Z. Li, and Y. Cheng, Coupling of N_2^+ rotational states in an air laser from tunnel-ionized nitrogen molecules, Phys. Rev. A **90**, 042504 (2014).

[31] H. Lei, G. Li, H. Xie, Q. Zhang, X. Wang, J. Zhao, Z. Chen, and Z. Zhao, Mechanism and control of rotational coherence in femtosecond laser-driven N_2^+, Opt. Express **28**, 22829 (2020).

[32] M. Britton, M. Lytova, D. H. Ko, A. Alqasem, P. Peng, D. M. Villeneuve, C. Zhang, L. Arissian, and P. B. Corkum, Control of N_2^+ air lasing, Phys. Rev. A **102**, 053110 (2020).

[33] S. R. Langhoff, C. W. Bauschlicher, and H. Partridge, Theoretical study of the N_2^+ Meinel system, J. Chem. Phys. **87**, 4716 (1987).

[34] S. R. Langhoff and C. W. Bauschlicher, Jr., Theoretical study of the first and second negative systems of N_2^+, J. Chem. Phys. **88**, 329 (1988).

[35] S.-F. Zhao, C. Jin, A.-T. Le, T. F. Jiang, and C. D. Lin, Determination of structure parameters in strong-field tunneling ionization theory of molecules, Phys. Rev. A **81**, 033423 (2010).

[36] J. M. Brown and A. Carrington, *Rotational Spectroscopy of Diatomic Molecules* (Cambridge University Press, Cambridge, 2003).

[37] Y. R. Liu, Y. Wu, J. G. Wang, O. Vendrell, V. Kimberg, and S. B. Zhang, Electron-rotation coupling in diatomics under strong-field excitation, Phys. Rev. A **102**, 033114 (2020).

[38] F. Anis and B. D. Esry, Role of nuclear rotation in dissociation of H_2^+ in a short laser pulse, Phys. Rev. A **77**, 033416 (2008).